The Astrophysical Journal, 792:41 (7pp), 2014 September 1 doi:10.1088/0004-637X/792/1/41

OSCILLATIONS IN A SUNSPOT WITH LIGHT BRIDGES

Ding Yuan[1,2,3], Valery M. Nakariakov[4,5,6], Zhenghua Huang[2], Bo Li[2], Jiangtao Su[1], Yihua Yan[1], and Baolin Tan[1]
[1] Key Laboratory of Solar Activity, National Astronomical Observatories, Chinese Academy of Sciences, Beijing 100012, China; Ding.Yuan@wis.kuleuven.be
[2] School of Space Science and Physics, Shandong University, Weihai 246209, China
[3] Centre for mathematical Plasma Astrophysics, Department of Mathematics, KU Leuven, Celestijnenlaan 200B bus 2400, B-3001 Leuven, Belgium
[4] Centre for Fusion, Space and Astrophysics, Department of Physics, University of Warwick, Coventry CV4 7AL, UK
[5] School of Space Research, Kyung Hee University, Yongin, 446-701 Gyeonggi, Korea
[6] Central Astronomical Observatory of the Russian Academy of Sciences at Pulkovo, 196140 St Petersburg, Russia
Received 2014 April 16; accepted 2014 July 10; published 2014 August 13

ABSTRACT

The Solar Optical Telescope on board *Hinode* observed a sunspot (AR 11836) with two light bridges (LBs) on 2013 August 31. We analyzed a two-hour Ca II H emission intensity data set and detected strong five-minute oscillation power on both LBs and in the inner penumbra. The time–distance plot reveals that the five-minute oscillation phase does not vary significantly along the thin bridge, indicating that the oscillations are likely to originate from underneath it. The slit taken along the central axis of the wide LB exhibits a standing wave feature. However, at the center of the wide bridge, the five-minute oscillation power is found to be stronger than at its sides. Moreover, the time–distance plot across the wide bridge exhibits a herringbone pattern that indicates a counter-stream of two running waves, which originated at the bridge's sides. Thus, the five-minute oscillations on the wide bridge also resemble the properties of running penumbral waves. The five-minute oscillations are suppressed in the umbra, while the three-minute oscillations occupy all three cores of the sunspot's umbra, separated by the LBs. The three-minute oscillations were found to be in phase at both sides of the LBs. This may indicate that either LBs do not affect umbral oscillations, or that umbral oscillations at different umbral cores share the same source. It also indicates that LBs are rather shallow objects situated in the upper part of the umbra. We found that umbral flashes (UFs) follow the life cycles of umbral oscillations with much larger amplitudes. They cannot propagate across LBs. UFs dominate the three-minute oscillation power within each core; however, they do not disrupt the phase of umbral oscillation.

Key words: magnetohydrodynamics (MHD) – Sun: atmosphere – Sun: chromosphere – Sun: oscillations – sunspots – waves

Online-only material: color figures

1. INTRODUCTION

Waves and oscillations in sunspots are some of the most extensively studied magnetohydrodynamic (MHD) wave phenomena in solar physics (see a comprehensive review by Bogdan & Judge 2006). The associated MHD seismology is a potential tool to probe a sunspot's thermal and magnetic structure (e.g., Zhugzhda et al. 1983; Zhugzhda 2008; Shibasaki 2001; Yuan et al. 2014), and photospheric–coronal magnetic connectivity (Sych et al. 2009; Yuan et al. 2011). The oscillation power distribution of different periods in a sunspot is nonuniform in both horizontal and vertical directions. The three-minute oscillations dominate a sunspot's umbra in the chromosphere, while the five-minute oscillations are most prominent in the penumbra (see, e.g., Bogdan & Judge 2006; Yuan et al. 2014).

Umbral oscillations are usually interpreted as standing slow mode magnetoacoustic waves (e.g., Christopoulou et al. 2000, 2001; Botha et al. 2011). The emission intensity and Doppler velocity inside sunspot umbrae oscillate collectively with a period of about three minutes, reaching the maximum amplitudes at the chromospheric heights (e.g., Reznikova et al. 2012; Yuan et al. 2014). The effect of height inversion occurs in the umbral oscillation power: a hump in the oscillation power is usually found at chromospheric heights; however, a power depletion is usually detected at photospheric heights underneath (Kobanov et al. 2011). Aballe Villero et al. (1993) found a clear correlation between three-minute oscillation power and umbral brightness in the dark core. In the corona, the three-minute oscillations become propagating slow magnetoacoustic waves and follow the magnetic fan structures extending out from the sunspot (De Moortel et al. 2002a, 2002b; De Moortel 2009; Botha et al. 2011; Yuan & Nakariakov 2012; Kiddie et al. 2012).

Umbral flashes (UFs; Beckers & Tallant 1969) are seen as strong brightenings occurring at seemingly random locations in sunspot umbrae. Their repetition rate is about two to three minutes, indicating their possible connection with umbral oscillations (Rouppe van der Voort et al. 2003; de la Cruz Rodríguez et al. 2013). Chromospheric UFs are proposed to be magnetoacoustic shock fronts produced by the photospheric sound waves (Havnes 1970), which is consistent with the sawtooth waveform of the UF trains (see, e.g., Tian et al. 2014). Bard & Carlsson (2010) performed one-dimensional radiative hydrodynamic simulations and demonstrated that UFs are enhanced emissions of local plasma during the passage of photospheric acoustic waves. High-resolution spectrometric studies appear to support this theory (e.g., Tziotziou et al. 2002, 2006, 2007; Rouppe van der Voort et al. 2003; de la Cruz Rodríguez et al. 2013). Socas-Navarro et al. (2000a, 2000b) detected anomalous Stokes spectra in conjunction with UF occurrences and claimed that UFs were associated with hot up-flowing material and a rest cool component. Moreover, Socas-Navarro et al. (2009) found rich fine structures of UFs and measured an unusually high lateral propagating speed that exceeded local fast speed, excluding the naive explanation of UF in terms of propagating fast magnetoacoustic waves. Thus, there remain a number of open questions associated with the specific details of UF physics.

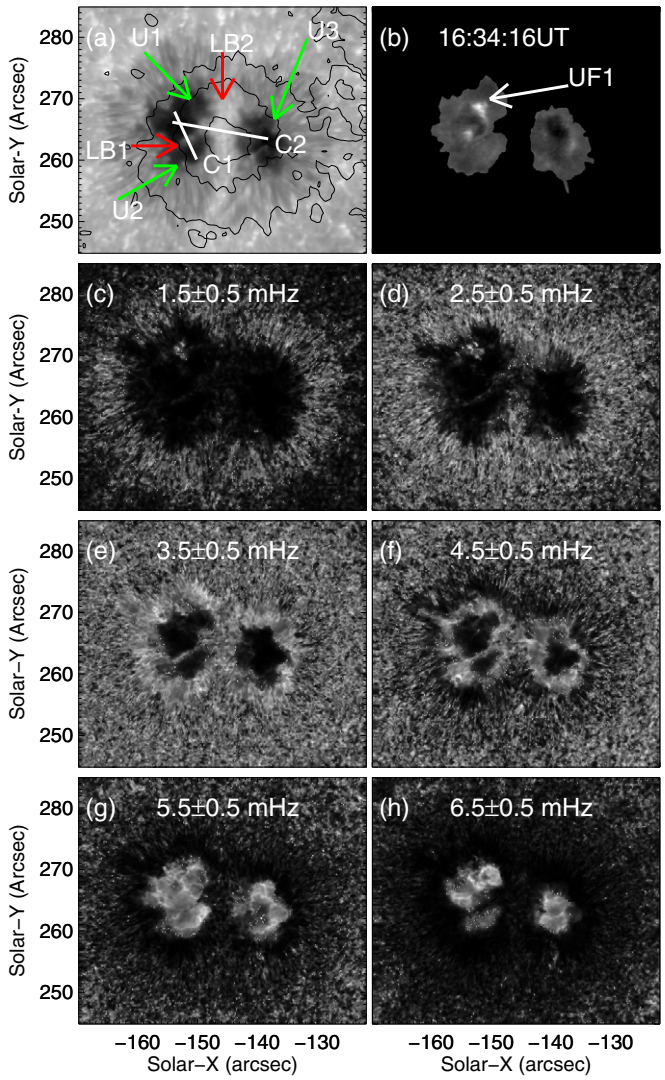

Figure 1. (a) SOT Ca II H emission intensity image of AR 11836, in a logarithmic scale. Faint and strong light bridges (LB1 and LB2) divide the sunspot umbra into three parts: U1, U2, and U3. The HMI magnetogram (contour) illustrates that all three parts of the umbra are of the same magnetic polarity. Two cuts across the light bridges, used in the following analysis, are annotated as C1 and C2. (b) A Ca II H difference image exhibiting the spatial extent of UF1, only the umbral region is shown. (c)–(h) The normalized narrow-band Fourier power maps averaged over 1 mHz bands around the central frequencies. The central frequencies of the spectral bands are labeled in each panel.

(A color version of this figure is available in the online journal.)

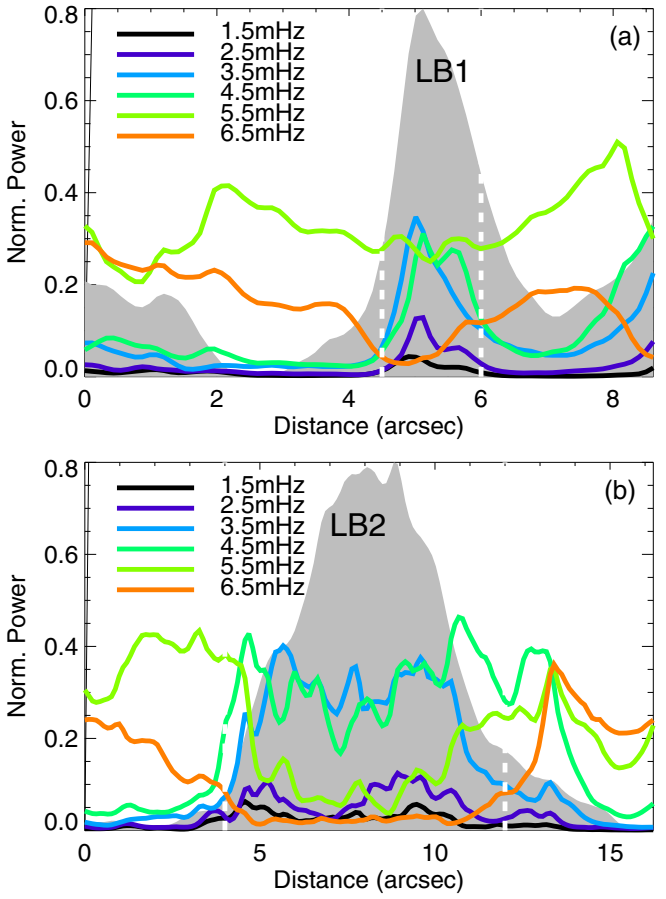

Figure 2. Profiles of the oscillation power profiles along cuts (a) C1 and (b) C2 for different frequency bands. The positions of LB1 and LB2 are shown by the scaled intensity variations (gray shade) along C1 and C2.

(A color version of this figure is available in the online journal.)

Longer period spectral components, commonly known as five-minute oscillations, are usually suppressed inside umbrae (Zirin & Stein 1972). Significant oscillation power forms a ring structure at the umbra–penumbra boundary, with the radius of the rings increasing with the increase in the oscillation period (Nagashima et al. 2007; Sych & Nakariakov 2008; Reznikova et al. 2012; Yuan et al. 2014). The physical mechanism responsible for such a behavior is still unclear. The solar *p*-mode acoustic wave is a candidate energy source (Abdelatif et al. 1986; Jain et al. 2009; Parchevsky & Kosovichev 2009). In particular, the interaction of *p* modes with the strong magnetic field in a sunspot could excite magnetoacoustic modes (Cally & Bogdan 1997; Cally et al. 2003; Schunker & Cally 2006; Khomenko & Calvo Santamaria 2013). Penn & Labonte (1993) suggested that *p*-mode absorption by sunspots occurs linearly across a sunspot umbra or within a ring surface where the local magnetic field allows for the optimized absorption rate. Moreover, such ring-surface absorption is favored in theoretical studies (Cally et al. 2003; Schunker & Cally 2006), with the *p*-mode absorption found to be optimal at an attack angle of about 30°.

The penumbral magnetic field deviates gradually from the solar normal with the distance from the umbra–penumbra border and becomes almost horizontal at the supra-penumbra (Borrero & Ichimoto 2011; Solanki 2003). Thus, the relatively simple magnetic geometry of the umbral and penumbral magnetic field allows for the development of relatively simple models describing sunspot oscillations and their application in observations. However, there are fine details such as umbral dots and light bridges (LBs) in umbrae. LBs are usually seen as bright extended filaments across the umbrae. The magnetic structure of LBs is believed to be rather different from the almost vertical and uniform field in the umbrae. It is likely to form a magnetic canopy with a large horizontal component (Rueedi et al. 1995; Leka 1997; Jurčák et al. 2006). Sunspot oscillations have not been investigated against such magnetic topology. However, bright umbral structures, such as dots and LBs, were numerically demonstrated to deteriorate sunspot oscillations, and hence reveal further physics (Locans et al. 1988). Recently, Sobotka et al. (2013) performed an analysis of oscillations in a pore with an LB, but without a penumbra, and found that the oscillations in the LB were very different from the usual three-minute oscillations in the umbral part of the pore.

In this study, we present a high-cadence and fine-resolution observation of oscillations in a well-developed sunspot with

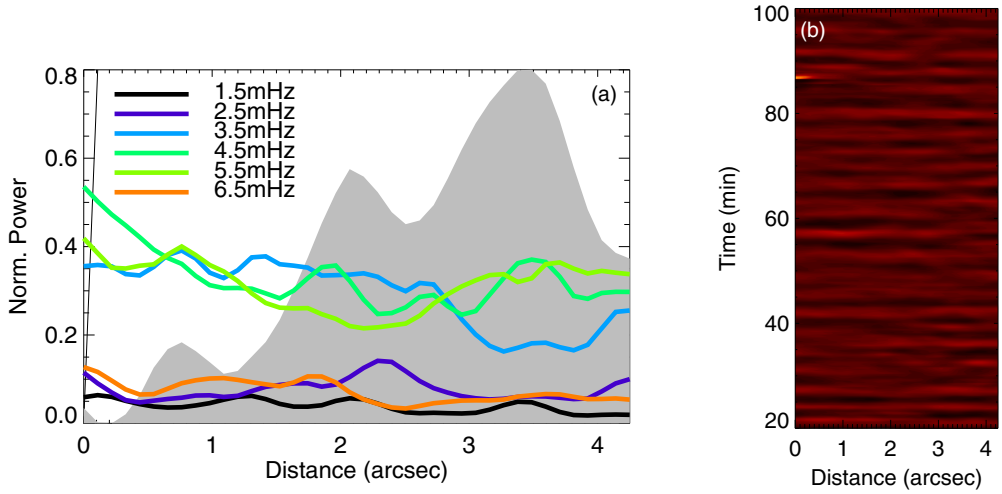

Figure 3. (a) Narrow-band power profiles along LB1 in different frequency bands. The gray shade denotes the emission intensity variation along the axis of the bridge. (b) The time–distance plot along LB1 in the baseline-difference array.

(A color version of this figure is available in the online journal.)

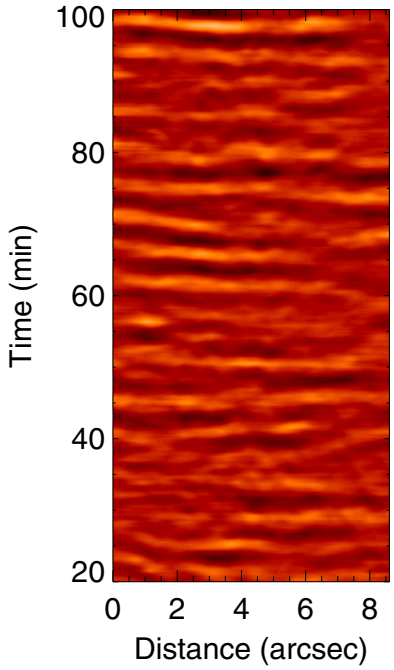

Figure 4. Time–distance plot along LB2 in the baseline-difference array.

(A color version of this figure is available in the online journal.)

two LBs of different width, at the chromospheric level. We focus on the spatial distribution of three-minute, including UFs, and five-minute oscillations in the sunspot's umbra and LBs, investigating how LBs affect umbral oscillations. We present data preparation in Section 2, analysis and results in Section 3, and conclusions in Section 4.

2. OBSERVATIONS

The Solar Optical Telescope (SOT; Tsuneta et al. 2008) on board the *Hinode* satellite (Kosugi et al. 2007) observed the chromosphere of a divided sunspot AR 11836 on 2013 August 31. A faint LB and a strong LB (labeled LB1 and LB2, respectively) divided the umbra into three cores of the same magnetic polarity (U1, U2, and U3; see Figure 1(a)). LB2 was a strong photospheric (granular) bridge (Muller 1979; Sobotka et al. 1994) and was observed by both the SOT's Ca II H (3968.5 Å) bandpass and *G* band.[7] It was formed before AR 11836 first became observable on the solar disk on August 28, faded off, accompanying the shrinking of umbral core U3, and disappeared on September 2, according to the continuous observation with the *Solar Dynamic Observatory* (*SDO*; Pesnell et al. 2012). It is a typical splitting process when a main spot is crossed by a wide granular bridge (Vazquez 1973). LB1 was an umbral streamer (Muller 1979), also visible in both of the SOT's bandpasses; however, its evolution was hardly resolved with the *SDO*.

The SOT's Broadband Filter Imager obtained a series of 512×512 pixels filtergrams in the Ca II H bandpass from 16:00 to 18:00 UT on 2013 August 31. The cadence was about 15 s and the pixel size was approximately 0.1 arcsec. The SolarSoft routine *fg_prep.pro* calibrated the fits images by subtracting the dark current, applying a flat field, correcting the bad pixels, and normalizing them with their exposure times. The SOT images were then reframed onto the Helioseismic and Magnetic Imager (HMI on board *SDO*; Schou et al. 2012) image coordinates by matching the sunspot centers. We tracked a $48'' \times 40''$ region against the solar differential rotation and obtained a sequence of images of 441×368 pixels in size. The images were co-aligned by compensating the offsets obtained by the cross-correlation technique and were interpolated into a uniform time grid with a 15 s cadence. We detrended and normalized the images with 20 points running mean values and obtained a baseline-ratio difference image set (see the technique details in, e.g., Aschwanden & Schrijver 2011; Yuan & Nakariakov 2012).

3. ANALYSIS AND RESULTS

We first examined the spatial distribution of the oscillation power over the sunspot. A fast Fourier transform (FFT) was applied pixel-by-pixel to the baseline-ratio difference array. Time series of each pixel was apodized with a Tukey window with $\alpha = 0.2$ (Harris 1978) before FFT to mitigate the effect of a finite observation interval. The obtained power maps were

[7] *G*-band observations over AR 11836 do not have good cadence for this study, thus they are not used.

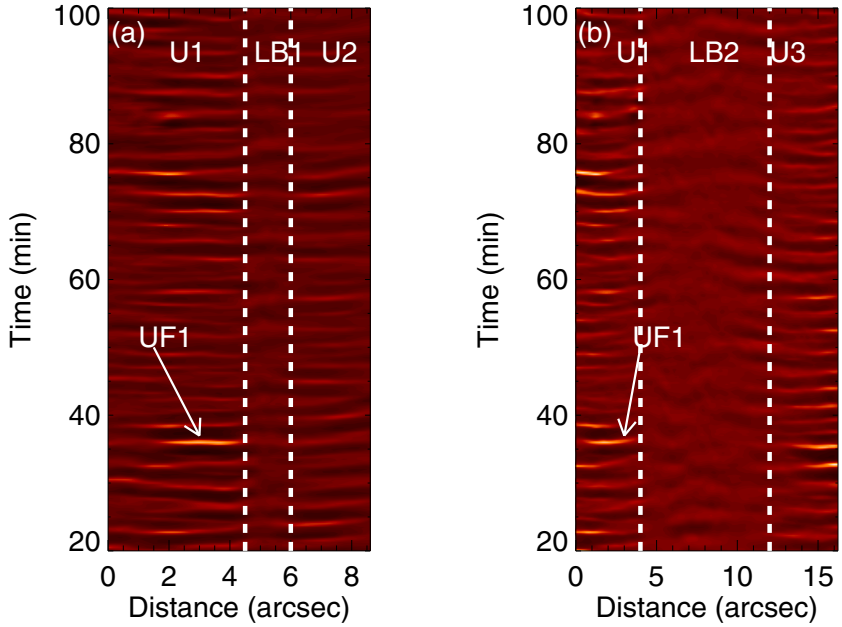

Figure 5. Time–distance plot of cuts (a) C1 and (b) C2. The approximate positions of LB1 and LB2 are enclosed by dashed lines. UF1 is labeled in each panel. (A color version of this figure is available in the online journal.)

normalized with their maximum power. Figure 1(c)–(h) display the normalized narrow-band power maps averaged over 1 mHz bands and centered at the frequencies of 1.5, 2.5, ⋯, and 6.5 mHz. Figure 1 clearly shows that high-frequency oscillations fill the umbrae, while the low-frequency counterparts take up the penumbra. This result is consistent with previous studies (e.g., Nagashima et al. 2007; Reznikova & Shibasaki 2012; Jess et al. 2013; Yuan et al. 2014).

3.1. Oscillations on Light Bridges

LBs are seen to be filled in with the oscillation power at frequencies of 3.5 mHz and 4.5 mHz (the five-minute band, Figure 1), but devoid of 5.5 mHz and 6.5 mHz oscillation power (the three-minute band). To illustrate this effect, we took the power profiles along cuts C1 and C2 that cross LB1 and LB2, respectively (see Figure 2). It is clear that oscillation powers of 3.5 mHz and 4.5 mHz exhibit humps in the LBs, while those of 5.5 mHz and 6.5 mHz are depleted in the LBs. LBs in pores were found to exhibit a similar feature (Sobotka et al. 2013).

Sources of five-minute oscillations on the faint bridge supposedly are either laterally at the penumbral ends of the bridge or come from underneath. In the former case, we expect an edge-to-center variation of five-minute oscillation power and phase along the bridge. We took the power profiles of the oscillations along LB1, shown in Figure 3(a). No clue proves that the bridge ends have stronger five-minute oscillations than the center. Moreover, the time–distance plot made along LB1 (Figure 3(b)) reveals no propagating features. Therefore, the five-minute oscillations are more likely to originate from underneath, rather than coming on the bridge from its ends anchored in the penumbra, and exhibit features of standing slow magnetoacoustic wave.

LB2 is stronger and wider than LB1, thus its fine structure may reveal more physics. The time–distance plot along LB2 (Figure 4) exhibits similar standing wave features as observed along LB1. The LB2 part of the time–distance plot along C2 (normal to LB2, Figure 5(b)) exhibits a weak herringbone pattern, indicating a counter stream of running waves from two

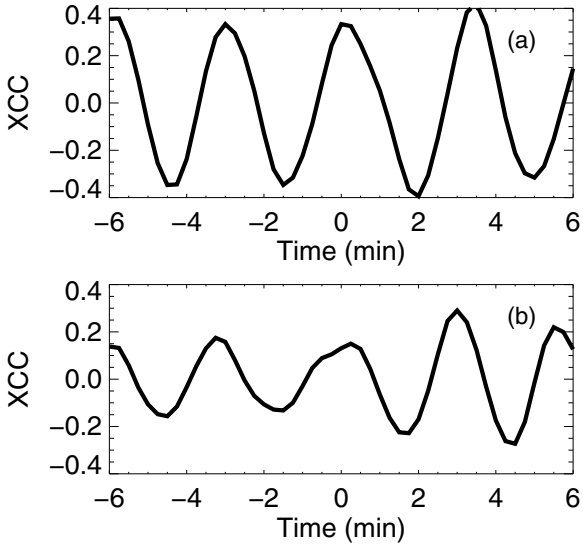

Figure 6. Cross-correlation coefficient (XCC) of the time series averaged at two sides of (a) LB1 and (b) LB2, respectively, as a function of lag time.

umbral cores, U1 and U3. The apparent propagation speed is about 10–20 km s^{-1}. Moreover, the 3.5 and 4.5 mHz oscillation power is slightly lower at the LB2's center than those at its sides (Figure 2(b)). We observe waves propagating inwardly from the bridge's long sides to its central axis. In the direction along the central axis of the bridge, we see a standing wave.

3.2. Oscillations Around Light Bridges

The three-minute oscillations were delimited by umbral boundaries and LBs (Figure 1). Figure 5 displays a segment of the time–distance maps along C1 and C2 in the baseline-ratio difference array. The horizontal ridges seen in the time–distance plots are well-consistent with the interpretation in terms of standing slow magnetoacoustic waves (see, e.g., Christopoulou et al. 2000, 2001; Botha et al. 2011). The wave fronts on

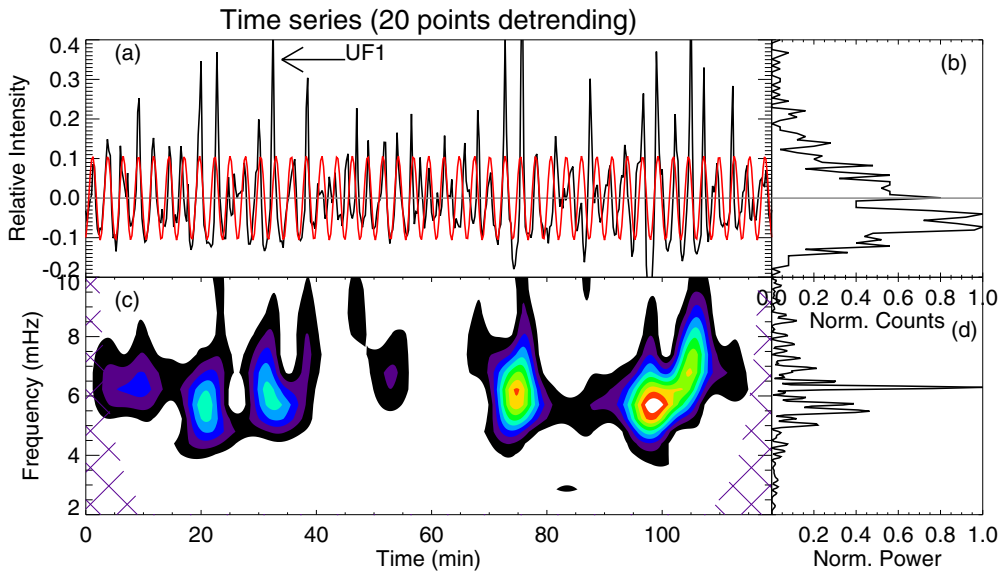

Figure 7. (a) Baseline-ratio intensity variation of a pixel taken at U1. The red curve is a single harmonic fit to the time series. Other panels are (b) the histogram of time series, (c) the Morlet wavelet spectrum, and (d) the periodogram.

(A color version of this figure is available in the online journal.)

both sides of an LB appear to have almost a one-to-one correspondence. To quantify this effect, we selected the U1 and U2 parts (located at 0–4.″0 and 6.″0–8.″6, respectively) of the time–distance array along cut C1 (see the dashed lines in Figure 5(a)), and obtained two time series by averaging the selected partial time–distance arrays over the space domain. We calculated the cross-correlation coefficient (XCC) of the two time series for different lag times; see Figure 6(a). Thresholding was applied at a value of 0.2 to mitigate the effect of the spikes introduced by UFs. The first maximum of the XCC was detected at a zero lag time. This means that the umbral oscillations at both sides of LB1 are apparently in phase. We applied the same analysis to the U1 (0″–4″) and U3 (12″–16.″4) parts of the time–distance map along C2 and obtained that the time lag corresponding to the maximum correlations is about 15 s. As this value is about the cadence time of the measurements, see Figure 6(b), and much shorter than the oscillation period, hence it could also be considered as a zero lag time. Therefore, our analysis reveals that the umbral oscillations in U1, U2, and U3 are apparently in phase, although the spatial locations of these oscillations are separated by LBs.

3.3. Umbral Flashes

Apart from the quasi-monochromatic oscillations discussed above, the observed sunspot hosts interesting examples of UF phenomenon. UFs are seen as local emission intensity enhancements in chromospheric umbrae (see Figure 1(b)) of the analyzed sunspot. This phenomenon is illustrated by UF1 as an example: its spatial extent (Figure 1(b)), its spatiotemporal morphology (Figure 5), and its time profile (Figure 7(a)).

We see that UFs occur as trains of several sharp increases in the brightness. Inside the trains, the UFs repeat with a three-minute periodicity that is consistent with the early findings (see, e.g., Rouppe van der Voort et al. 2003; de la Cruz Rodríguez et al. 2013). Figure 5 reveals that the UF trains occur at random locations without a well-established occurrence rate. Moreover, individual UFs are seen to ride wave fronts of umbral oscillations. However, in contrast to the apparent coherence of the three-minute oscillations on either sides of LBs discussed in Section 3.2, UFs lack the one-to-one correspondence at either sides of LBs (see Section 3.2). Thus, UFs are confined within the umbral cores and cannot propagate across LBs.

Figure 7 plots the time series of a pixel in the U1 part of C2 and its power spectrum. The amplitude of umbral oscillations is normally less than 10% of the background intensity, but surges up to 60% when an UF occurs. The series of spikes introduced by UFs constitute the major oscillation power in the wavelet spectrum (Figure 7(c)) and contribute significantly to the peak at about 6.2 mHz in the periodogram (Figure 7(d)). Between UFs, umbral oscillations produce minor power in comparison with UF oscillations in spite of their persistence over the whole time series.

The time series of the intensity variation were over-plotted with a sinusoidal fit (red curve, Figure 7(a)). This figure confirms the finding that UFs follow the cycles of umbral oscillations (also see Figure 5) and that UFs do not disrupt the phase of three-minute oscillations. Thus, we see that UFs' intensity variation (Figure 7(a)) exhibits no significant difference with three-minute oscillations in the umbra, apart from having a much larger amplitude, at about 50% of the background intensity.

4. CONCLUSIONS

We have analyzed the intensity variations in a sunspot AR 11836 with two LBs, observed with *Hinode*/SOT in the Ca II H bandpass. In full agreement with commonly accepted knowledge, the three-minute oscillations were found to occupy the umbral part of the sunspot, while five-minute oscillations fill in the penumbra. Our narrow-band power map analysis shows that significant five-minute oscillations are also present in LBs, while three-minute oscillations are suppressed there. Our finding generalizes the earlier results recently obtained by Sobotka et al. (2013) for a pore in the case of a well-developed sunspot with a penumbra. The five-minute oscillation power along the faint bridges (LB1) does not exhibit recognizable features, however, the time–distance plot along LB1 illustrated that the five-minute oscillations do not experience a noticeable change in the phase along the bridge. Thus, five-minute oscillations are

found to exhibit a standing wave behavior along the thin bridge (Figure 3), the same process was found along the central axis of LB2 (Figure 4).

We should address the concern that the contamination of stray light could generate a spurious signal and affect the subsequent analysis, since LB1 is measured to be less than 2″ wide and about 4″ long. In the discussed case, however, this effect is negligible, since LB1 was surrounded by umbrae that were much darker. Moreover, if the stray light did contribute significantly to the emission of LB1, we would expect to observe significant three-minute oscillations associated with the umbral oscillations, in the LB. However, our analysis did not show the presence of three-minute oscillations in the LBs.

The five-minute oscillations on the strong bridge (LB2) show a rather complex behavior. The time–distance plot across LB2 exhibits a weak herringbone pattern that denotes two waves running toward each other from the opposite sides of the bridge. The projected propagation speed is about 10–20 km s^{-1}. Because this value is about the typical value found for running penumbral waves, and because the waves are seen to propagate in the direction perpendicular to the LB sides, it may be considered to be an LB counterpart of the running penumbral wave phenomenon. This finding may indicate that the wave carries energy from the umbral cores inward toward the LB. However, one should be cautious with this interpretation, since the apparent wave motion may not be associated with any energy transfer. Indeed, what is measured is the phase speed, which does not represent any energy transfer, and the apparent wave motion can be caused by, e.g., the projection of the waves propagating along the magnetic field lines. Our finding demonstrates the need for a more detailed study of this effect.

The suppression of three-minute oscillations in the LB can be associated with the departure of the magnetic field lines from the vertical over the bridge. Indeed, if in the chromosphere above an LB, the field has a canopy geometry (see, e.g., the illustration shown in Figure 7 of Jurčák et al. 2006). Thus, the LB effect on MHD waves should be similar to this of the umbra–penumbra boundary, and hence the resonant properties of the LB and of the umbra–penumbra boundary should be similar. This results in the observed suppression of three-minute oscillations and the appearance of five-minute oscillations at both LB and umbra–penumbra boundaries. However, there is an important issue connected with the excitation of the five-minute oscillations in LBs. The well-developed theory of the *p*-mode absorption by sunspots (Cally et al. 2003; Schunker & Cally 2006; Jain et al. 2009; Khomenko & Calvo Santamaria 2013) should answer the question of how the acoustic oscillations come to the LB. To illustrate this problem, consider an LB as the top of a vertical magnetic-free (or almost magnetic-free) slab surrounded by the strong umbral magnetic field. The top boundary of the slab is formed by the magnetic canopy. The *p* modes surrounding the sunspot cannot penetrate the LB through the long sides formed by the umbral magnetic field. Thus, there are two possibilities, the *p* modes either enter the LB through its ends or from underneath. In either case, the angular spectrum of the *p* modes that can reach the LB is very restricted. This could possibly be seen in the observations, either as a significant decrease in the five-minute oscillation power in the LB in comparison with the umbra–penumbra boundary, or as the formation of waves propagating along the bridge and carrying the five-minute energy to its center. Neither effect was detected by our analysis in the thin bridge: the spatial structure of five-minute oscillations at the umbra–penumbra boundary and at the LBs is similar. However, there is clear evidence of the waves propagating from the sides of the wide bridge toward its center. Thus, modeling of the *p*-mode interaction with a sunspot that has an LB is an interesting topic for theoretical consideration.

In addition, our analysis showed that three-minute umbral oscillations at both sides of both the wide and thin LBs are in-phase. Perhaps, this effect is associated with the excitation of the three-minute umbral oscillations on the either side of the LB by the same source that apparently "does not feel" the LB, or with some cross-talk of the three-minute oscillations occurring at the neighboring (while separated by the LB) spatial locations. It implies that LBs are shallow objects situated in the upper part of the umbra. The umbral cores are probably connected below the LB surface. In this scenario, the standing waves observed in bridges are not connected with *p* modes, as they are not likely to reach the bridges because of the surrounding umbra. This suggests that five-minute standing oscillations in LBs are possibly standing acoustic oscillations trapped in the vertical nonuniformity of the plasma density and temperature along the magnetic field (Zhugzhda 2008; Botha et al. 2011). Also, the possibility of a mere coincidence cannot be ruled out, and more observational examples need to be studied to assess the statistical significance of this finding.

The parts of the umbra separated by LBs showed transient UFs. The UFs were found to follow the cycles of umbral three-minute oscillations and do not disrupt their phase. Thus, UFs are seen to be high amplitude parts of the amplitude-modulated three-minute oscillations (see Sych et al. 2012, for the discussion of the modulation of three-minute umbral oscillations). In UFs, the amplitude of three-minute oscillations reaches 60% of the background intensity and dominates in the three-minute spectral peak. The finite-amplitude (weakly nonlinear) effects naturally lead to the wave steepening and the formation of acoustic shocks. UFs were found to be constrained within an umbral core. In contrast with the three-minute oscillations discussed above, UFs on both sides of the LBs did not show significant correlations.

This work is supported by the Marie Curie PIRSES-GA-2011-295272 *RadioSun* project, the European Research Council under the *SeismoSun* Research Project No. 321141 (D.Y. and V.M.N.), the Open Research Program KLSA201312 of the Key Laboratory of Solar Activity of the National Astronomical Observatories of China (D.Y.), the Russian Foundation of Basic Research under grant 13-02-00044; the BK21 plus program through the National Research Foundation funded by the Ministry of Education of Korea (V.M.N.), the National Natural Science Foundation of China (40904047, 41174154, and 41274176), the Ministry of Education of China (20110131110058 and NCET-11-0305), the Provincial Natural Science Foundation of Shandong via Grant JQ201212 (B.L., D.Y.), the China 973 program 2012CB825601, NSFC Grants 41274178 (Z.H.H.), 11373040 (J.T.S.), 11273030, 11221063, and MOST Grant 2011CB811401 (B.L.T., Y.H.Y.).

Facility: Hinode (SOT)

REFERENCES

Aballe Villero, M. A., Marco, E., Vazquez, M., & Garcia de La Rosa, J. I. 1993, A&A, 267, 275
Abdelatif, T. E., Lites, B. W., & Thomas, J. H. 1986, ApJ, 311, 1015
Aschwanden, M. J., & Schrijver, C. J. 2011, ApJ, 736, 102
Bard, S., & Carlsson, M. 2010, ApJ, 722, 888
Beckers, J. M., & Tallant, P. E. 1969, SoPh, 7, 351
Bogdan, T. J., & Judge, P. G. 2006, RSPTA, 364, 313

Borrero, J. M., & Ichimoto, K. 2011, LRSP, 8, 4
Botha, G. J. J., Arber, T. D., Nakariakov, V. M., & Zhugzhda, Y. D. 2011, ApJ, 728, 84
Cally, P. S., & Bogdan, T. J. 1997, ApJL, 486, L67
Cally, P. S., Crouch, A. D., & Braun, D. C. 2003, MNRAS, 346, 381
Christopoulou, E. B., Georgakilas, A. A., & Koutchmy, S. 2000, A&A, 354, 305
Christopoulou, E. B., Georgakilas, A. A., & Koutchmy, S. 2001, A&A, 375, 617
de la Cruz Rodríguez, J., Rouppe van der Voort, L., Socas-Navarro, H., & van Noort, M. 2013, A&A, 556, A115
De Moortel, I. 2009, SSRv, 149, 65
De Moortel, I., Hood, A. W., Ireland, J., & Walsh, R. W. 2002a, SoPh, 209, 89
De Moortel, I., Ireland, J., Walsh, R. W., & Hood, A. W. 2002b, SoPh, 209, 61
Harris, F. 1978, IEEEP, 66, 51
Havnes, O. 1970, SoPh, 13, 323
Jain, R., Hindman, B. W., Braun, D. C., & Birch, A. C. 2009, ApJ, 695, 325
Jess, D. B., Reznikova, V. E., Van Doorsselaere, T., Keys, P. H., & Mackay, D. H. 2013, ApJ, 779, 168
Jurčák, J., Martínez Pillet, V., & Sobotka, M. 2006, A&A, 453, 1079
Khomenko, E., & Calvo Santamaria, I. 2013, JPhCS, 440, 012048
Kiddie, G., De Moortel, I., Del Zanna, G., McIntosh, S. W., & Whittaker, I. 2012, SoPh, 279, 427
Kobanov, N. I., Kolobov, D. Y., Chupin, S. A., & Nakariakov, V. M. 2011, A&A, 525, A41
Kosugi, T., Matsuzaki, K., Sakao, T., et al. 2007, SoPh, 243, 3
Muller, R. 1979, SoPh, 61, 297
Leka, K. D. 1997, ApJ, 484, 900
Locans, V., Skerse, D., Staude, J., & Zhugzhda, I. D. 1988, A&A, 204, 263
Nagashima, K., Sekii, T., Kosovichev, A. G., et al. 2007, PASJ, 59, 631
Parchevsky, K. V., & Kosovichev, A. G. 2009, ApJ, 694, 573
Pesnell, W. D., Thompson, B. J., & Chamberlin, P. C. 2012, SoPh, 275, 3
Penn, M. J., & Labonte, B. J. 1993, ApJ, 415, 383
Reznikova, V. E., & Shibasaki, K. 2012, ApJ, 756, 35
Reznikova, V. E., Shibasaki, K., Sych, R. A., & Nakariakov, V. M. 2012, ApJ, 746, 119
Rouppe van der Voort, L. H. M., Rutten, R. J., Sütterlin, P., Sloover, P. J., & Krijger, J. M. 2003, A&A, 403, 277
Rueedi, I., Solanki, S. K., & Livingston, W. 1995, A&A, 302, 543
Schou, J., Scherrer, P. H., Bush, R. I., et al. 2012, SoPh, 275, 229
Schunker, H., & Cally, P. S. 2006, MNRAS, 372, 551
Shibasaki, K. 2001, ApJ, 550, 1113
Sobotka, M., Bonet, J. A., & Vazquez, M. 1994, ApJ, 426, 404
Sobotka, M., Švanda, M., Jurčák, J., et al. 2013, A&A, 560, A84
Socas-Navarro, H., McIntosh, S. W., Centeno, R., de Wijn, A. G., & Lites, B. W. 2009, ApJ, 696, 1683
Socas-Navarro, H., Trujillo Bueno, J., & Ruiz Cobo, B. 2000a, ApJ, 544, 1141
Socas-Navarro, H., Trujillo Bueno, J., & Ruiz Cobo, B. 2000b, Sci, 288, 1396
Solanki, S. K. 2003, A&ARv, 11, 153
Sych, R., Nakariakov, V. M., Karlicky, M., & Anfinogentov, S. 2009, A&A, 505, 791
Sych, R., Zaqarashvili, T. V., Nakariakov, V. M., et al. 2012, A&A, 539, A23
Sych, R. A., & Nakariakov, V. M. 2008, SoPh, 248, 395
Tian, H., DeLuca, E., Reeves, K. K., et al. 2014, ApJ, 786, 137
Tsuneta, S., Ichimoto, K., Katsukawa, Y., et al. 2008, SoPh, 249, 167
Tziotziou, K., Tsiropoula, G., Mein, N., & Mein, P. 2006, A&A, 456, 689
Tziotziou, K., Tsiropoula, G., Mein, N., & Mein, P. 2007, A&A, 463, 1153
Tziotziou, K., Tsiropoula, G., & Mein, P. 2002, A&A, 381, 279
Vazquez, M. 1973, SoPh, 31, 377
Yuan, D., & Nakariakov, V. M. 2012, A&A, 543, A9
Yuan, D., Nakariakov, V. M., Chorley, N., & Foullon, C. 2011, A&A, 533, A116
Yuan, D., Sych, R., Reznikova, V. E., & Nakariakov, V. M. 2014, A&A, 561, A19
Zhugzhda, I. D., Locans, V., & Staude, J. 1983, SoPh, 82, 369
Zhugzhda, Y. D. 2008, SoPh, 251, 501
Zirin, H., & Stein, A. 1972, ApJL, 178, L85